

Research



Cite this article: Wong SY, Wei Y, Mouritsen H, Solov'yov IA, Hore PJ. 2021 Cryptochrome magnetoreception: four tryptophans could be better than three. *J. R. Soc. Interface* **18**: 20210601.
<https://doi.org/10.1098/rsif.2021.0601>

Received: 22 July 2021

Accepted: 14 October 2021

Subject Category:

Life Sciences—Chemistry interface

Subject Areas:

biophysics

Keywords:

magnetoreception, cryptochrome, radical pairs, magnetic field effects, migratory songbirds

Author for correspondence:

P. J. Hore

e-mail: peter.hore@chem.ox.ac.uk

This article is dedicated to Professor Robert Kaptein (University of Utrecht) on the occasion of his 80th birthday.

Electronic supplementary material is available online at <https://doi.org/10.6084/m9.figshare.c.5677125>.

Cryptochrome magnetoreception: four tryptophans could be better than three

Siu Ying Wong¹, Yujing Wei², Henrik Mouritsen^{3,4}, Ilia A. Solov'yov¹ and P. J. Hore²

¹Institut für Physik, Carl-von-Ossietzky Universität Oldenburg, Oldenburg 26111, Germany

²Department of Chemistry, University of Oxford, Oxford OX1 3QZ, UK

³Institut für Biologie und Umweltwissenschaften, Carl-von-Ossietzky Universität Oldenburg, Oldenburg 26111, Germany

⁴Research Centre for Neurosensory Science, University of Oldenburg, Oldenburg 26111, Germany

id SYW, 0000-0002-1456-6000; HM, 0000-0001-7082-4839; IAS, 0000-0002-8626-145X; PJH, 0000-0002-8863-570X

The biophysical mechanism of the magnetic compass sensor in migratory songbirds is thought to involve photo-induced radical pairs formed in cryptochrome (Cry) flavoproteins located in photoreceptor cells in the eyes. In Cry4a—the most likely of the six known avian Crys to have a magnetic sensing function—four radical pair states are formed sequentially by the stepwise transfer of an electron along a chain of four tryptophan residues to the photo-excited flavin. In purified Cry4a from the migratory European robin, the third of these flavin–tryptophan radical pairs is more magnetically sensitive than the fourth, consistent with the smaller separation of the radicals in the former. Here, we explore the idea that these two radical pair states of Cry4a could exist in rapid dynamic equilibrium such that the key magnetic and kinetic properties are weighted averages. Spin dynamics simulations suggest that the third radical pair is largely responsible for magnetic sensing while the fourth may be better placed to initiate magnetic signalling particularly if the terminal tryptophan radical can be reduced by a nearby tyrosine. Such an arrangement could have allowed independent optimization of the essential sensing and signalling functions of the protein. It might also rationalize why avian Cry4a has four tryptophans while Crys from plants have only three.

1. Introduction

The remarkable magnetic compass sense that helps night-migratory songbirds navigate thousands of kilometres [1,2] is thought to have a photochemical mechanism [3–8]. The axial nature [1,9] and the light-dependence [10] of the birds' responses to the geomagnetic field, together with the involvement of the birds' visual system in processing magnetic compass information [11,12], are consistent with the formation of transient, magnetically sensitive radical pairs in photoreceptor cells in the retina [5]. The molecule that plays host to this photochemistry seems likely to be a member of the cryptochrome (Cry) family of proteins [13–15], a possibility first suggested more than 20 years ago [3]. Of the six known avian Crys [14,16–25], Cry1a and Cry4a are the main contenders (reviewed in [6,7]). There is also debate about whether the magnetically sensitive radical pairs are formed directly by photo-excitation of the protein or indirectly as intermediates during 'dark' back-reactions [26–32]. The identity of any 'dark' radical pair is unknown and vertebrate Cry1a does not seem to bind the crucial flavin adenine dinucleotide (FAD) chromophore at all strongly *in vitro* [33]. We focus here on Cry4a in which flavin–tryptophan radical pairs [34–38] arise from a series of electron transfers along a chain of aromatic amino acid residues that stretches approximately 25 Å from the FAD in the interior of the protein out to its surface [23,39]. In contrast to plant Crys, in which three

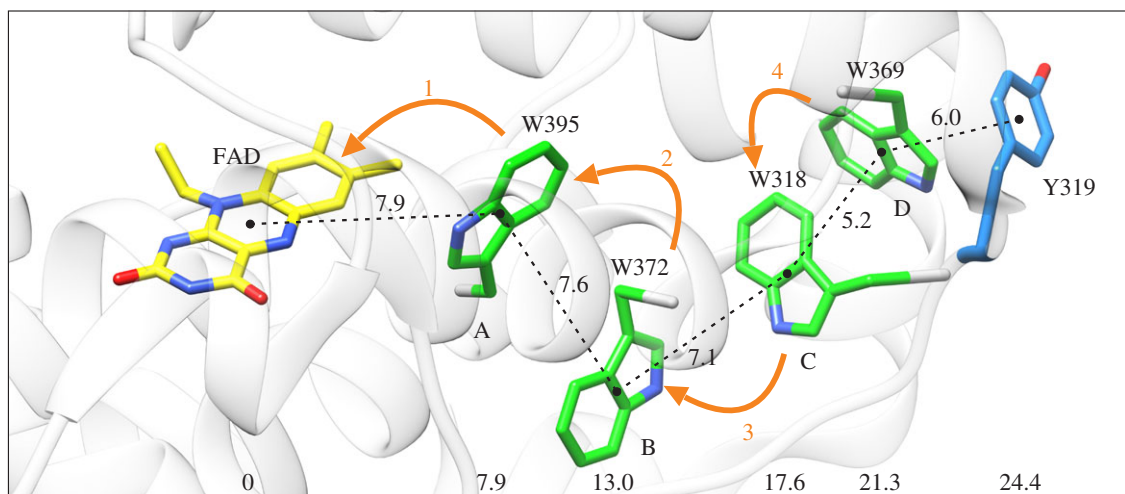


Figure 1. Structure of the electron transfer chain in *C/Cry4a* (PDB: 6PU0 [37]) showing the FAD chromophore, the tryptophan tetrad and Tyr319. The numbers between adjacent groups are centre-to-centre separations in Å. The numbers at the bottom of the figure are centre-to-centre distances from the FAD. The orange arrows indicate the four sequential electron transfers. Only the isoalloxazine part of the FAD is shown.

tryptophans (Trp), or two tryptophans and a tyrosine (Tyr), constitute the electron transfer pathway [13], animal and animal-like Crys possess a tetrad of tryptophans (e.g. avian Cry4s [23,39]) or three tryptophans plus a terminal tyrosine (e.g. *Chlamydomonas reinhardtii* Cry [40]).

Figure 1 shows the structure of the flavin component of the FAD and the four tryptophans (W) in pigeon (*Columba livia*, *Cl*) Cry4a, labelled: A (W395), B (W372), C (W318) and D (W369) [37]. The sequence numbers are the same for Cry4a from the night-migratory European robin (*Erithacus rubecula*, *Er*) [21]. Also shown is the sidechain of Tyr319, positioned at the far end of the Trp-tetrad, in contact with solvent. Photo-excitation of FAD in *ErCry4a* is followed by four consecutive electron transfers between adjacent donors/acceptors, producing four sequential radical pairs: $[FAD^{\bullet-} Trp_X H^{\bullet+}]$ (abbreviated $RP1_X$, $X = A, B, C$ or D) [39]. The separations of the flavin and tryptophan radicals in these four states of *ClCry4a* are approximately 8, 13, 18 and 21 Å, respectively [37]. Judging by molecular dynamics simulations, the electron transfer chain in *ErCry4a* has a very similar structure with very similar distances between the key components [39].

A recent study of purified robin Cry4a by Xu *et al.* [39], the first of its kind for any migratory animal Cry, has shed considerable light on the performance of the protein as a potential magnetoreceptor. Spectroscopic measurements were made on the wild-type (WT) protein, and four mutants, $W_X F$ ($X = A, B, C$ or D), in which each of the four tryptophans, in turn, had been replaced with phenylalanine (F) to block electron transfer at different points along the chain. The main findings are as follows. (i) Unlike some other avian Crys [33], *ErCry4a* can be purified with the essential FAD chromophore stoichiometrically bound. (ii) Blue-light irradiation of $W_A F$, $W_B F$ and $W_C F$ mutants either yielded no detectable radicals ($W_A F$) or produced FAD and Trp radicals that are too short-lived to be magnetically sensitive ($W_B F$ and $W_C F$). In the $W_D F$ mutant and the WT protein, however, light-induced radicals with lifetimes in excess of 100 ns were identified. (iii) From measurements of the radical–radical separations, it is clear that $RP1_D$ is the dominant transient charge-separated state in the WT protein. (iv) Smaller magnetic field effects were found for purified WT *ErCry4a* than for two proteins with only three

tryptophans: the $W_D F$ mutant of *ErCry4a* and Cry1 from the model plant, *Arabidopsis thaliana* (*AtCry1*) [39].

If Cry4a is the magnetic sensory molecule in migratory songbirds and if, *in vivo*, the $RP1_C$ state is more magnetically sensitive than $RP1_D$ (as is the case *in vitro*), then one might wonder why Cry4a has a Trp-tetrad instead of a Trp-triad. This is the question we address here. We explore the proposal [39] that, under the right conditions, a Trp-tetrad would be consistent with high detection sensitivity *and* might have allowed independent evolutionary optimization of the two essential functions of the protein—sensing and signalling. The key assumption underlying this idea is that $RP1_C$ and $RP1_D$ interconvert by fast reversible electron hopping, i.e. $FAD^{\bullet-} Trp_C H^{\bullet+} Trp_D H \leftrightarrow FAD^{\bullet-} Trp_C H Trp_D H^{\bullet+}$ [39].

2. Radical pair reaction schemes

Figure 2a shows part of the conventional Cry reaction scheme in the case that the magnetic field effect stems from a single radical pair ($RP1 = RP1_C$ or $RP1_D$) [41]. $RP1$ is formed by electron transfer along the tryptophan triad or tetrad to the photo-excited FAD (not shown) and interconverts coherently between its singlet ($^S RP1$) and triplet ($^T RP1$) states. At the same time, $^S RP1$ returns to the ground state (GS) by spin-selective back electron transfer (rate constant k_r ; r = recombination reaction) while both $^S RP1$ and $^T RP1$ can proceed to a stabilized radical pair state, $RP2$ (rate constant k_f ; f = forward reaction) [41]. In the latter step, a proton is lost from the indole nitrogen of the tryptophan radical, $TrpH^{\bullet+} \rightarrow Trp^{\bullet}$, to produce either $[FAD^{\bullet-} Trp_C^{\bullet}]$ ($RP2_C$) or $[FAD^{\bullet-} Trp_D^{\bullet}]$ ($RP2_D$). The magnetic field effect manifests as a change in the yield of $RP2$ and hence that of the signalling state (SS), a more stable form of the protein in which we assume the tryptophan radical has been reduced ($Trp^{\bullet} \rightarrow TrpH$) and the flavin radical protonated ($FAD^{\bullet-} \rightarrow FADH^{\bullet}$). SS then returns to the GS of the protein on a much longer timescale. We assume $RP2$ lives long enough *in vivo* (more than 10 μ s) that its electron spins are fully relaxed before conversion to SS so that it generates no additional magnetic field effects. In the simulations described below, we calculate the dependence of the quantum yield of SS (Φ_{SS} , assumed to equal

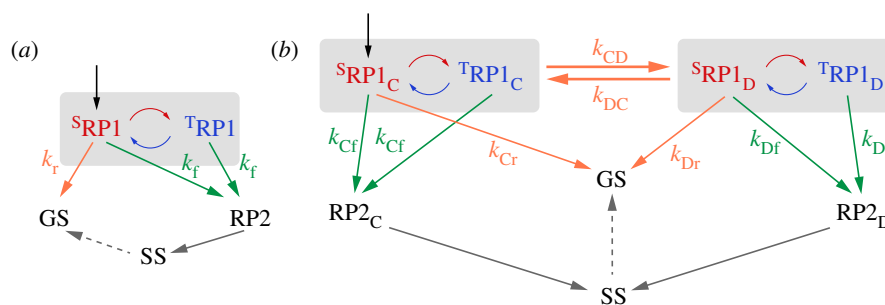


Figure 2. (a) Conventional reaction scheme in which magnetic field effects on the yield of the signalling state (SS) come from a single radical pair, RP1 (=RP1_C or RP1_D) [41]. Singlet and triplet states are labelled S and T, respectively. (b) Modified reaction scheme in which RP1_C and RP1_D both contribute to the magnetic field effect [39]. The vertical black arrows indicate the formation of singlet radical pairs by spin-conserving electron transfer along the Trp-triad or tetrad to the photo-excited singlet state of FAD. Orange arrows: electron transfer reactions. Green arrows: TrpH⁺ deprotonation reactions. Curved red/blue arrows: coherent singlet–triplet interconversion. The symbols beside the arrows are rate constants. GS denotes the ground state of the protein.

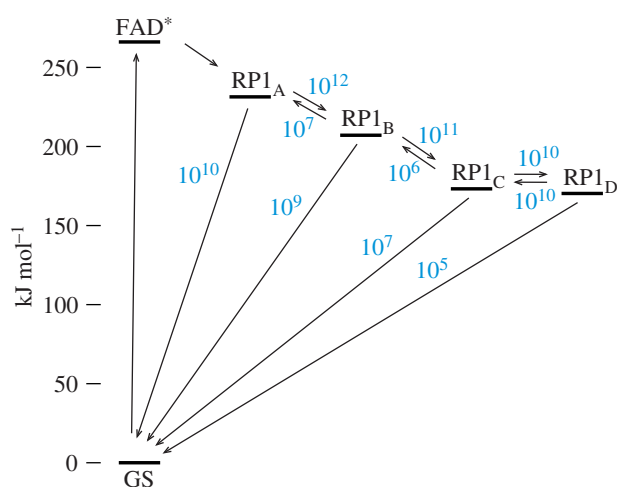


Figure 3. Approximate rate constants (in s⁻¹) for electron transfer reactions in ErCry4a. Values for RP1_A → GS and RP1_B → GS come from transient absorption experiments [39]. All other rate constants, and the free energies of the various states come from molecular dynamics simulations [39]. FAD* is the photo-excited singlet state of FAD. The RP2 and SS states are not shown.

that of RP2) on the direction of the external magnetic field with respect to an array of mutually aligned Cry molecules. This quantity represents the ‘signal’ from which a bird could derive a magnetic compass bearing. Conversion of GS to SS is thought to lead to a conformational change that alters the protein’s binding affinity to signalling partners and thereby initiates a biochemical signalling cascade [42].

The notion that RP1_C and RP1_D might jointly be responsible for the magnetic sensitivity of ErCry4a came from estimates of electron transfer rate constants (figure 3) derived from molecular dynamics simulations [39]. The first two steps along the chain of four tryptophans (RP1_A → RP1_B and RP1_B → RP1_C) were found to be rapid, exergonic and essentially irreversible. At each stage, forward electron transfer is two orders of magnitude faster than direct return to the GS, such that the RP1_C state would be formed in high yield. By contrast, RP1_C and RP1_D were found to have free energies differing by approximately $k_B T$ at physiological temperatures, with similar forward (k_{CD}) and backward (k_{DC}) electron transfer rate constants for the interconversion of the two states. The estimates of k_{CD} and k_{DC} (approx. 10^{10} s⁻¹ [39]), are considerably faster than both the singlet–triplet interconversion and the subsequent reactions of RP1_C and RP1_D, implying that both radical pairs may contribute to magnetic

sensing. We, therefore, explore a modified reaction scheme, figure 2b, involving the two interconverting radical pairs in which one electron spin is on the flavin and the other resides on either Trp_CH or Trp_DH [39]. The singlet states of both pairs can return to the GS (rate constants k_{Cr} and k_{Dr}) and the TrpH⁺ radicals can be deprotonated to form the RP2_C and RP2_D states (rate constants k_{Cf} and k_{Df}), which then proceed to the SS, again assumed to contain FADH^{*} as the only radical. In this modified reaction scheme, the yield of the SS, Φ_{SS} , remains the quantity of interest and is defined as the sum of the yields of RP2_C and RP2_D.

3. Methods

The reactions shown in figure 2b were modelled by means of coupled stochastic Liouville equations, one for each of the two states, RP1_C and RP1_D (see electronic supplementary material, section S1 for details). The spin Hamiltonians of the two radical pairs comprised electron Zeeman, electron–nuclear hyperfine and electron–electron dipolar interactions. Haberkorn operators were used for the recombination (k_{Cr} and k_{Dr}) and forward (k_{Cf} and k_{Df}) reaction steps [43]. Dipolar tensors [44] were calculated using the centre-to-centre vectors for FAD–Trp_C and FAD–Trp_D in ClCry4a [37]. The intensity of the geomagnetic field was 50 μ T in all simulations. The anisotropy of the quantum yield of the SS,

$$\Delta\Phi_{SS} = \max(\Phi_{SS}) - \min(\Phi_{SS}), \quad (3.1)$$

was calculated as a measure of the magnetic compass sensitivity, where Φ_{SS} is the sum of the yields of RP2_C and RP2_D. The maximum and minimum values of Φ_{SS} were determined by sampling, respectively, 1601 (figure 4) and 98 (figure 5) spherically distributed magnetic field directions. Note that this $\Delta\Phi_{SS}$ differs from the quantity plotted in figure 4c of Xu *et al.* [39] which is the change in the isotropic yield of the SS induced by a 50 μ T magnetic field, calculated using the reaction scheme in figure 2a.

Electron spin relaxation, with rate constant k_{relax} was included by modelling the effects of isotropic, randomly fluctuating local magnetic fields [45] (electronic supplementary material, equation S7). The rate of spin relaxation of radical pairs in Cry has not been determined experimentally. The best estimates of k_{relax} come from a study of Cry1 from the plant *A. thaliana*, using a combination of all-atom molecular dynamics simulations and Bloch–Redfield relaxation theory [45,46]. Librational motions of the FAD^{*} and TrpH⁺ radicals and fluctuations in their positions and dihedral angles modulate hyperfine and dipolar interactions and thereby induce spin relaxation at rates in the range 10^6 – 10^7 s⁻¹. The simulations described below were performed with $k_{relax} = 10^6$ s⁻¹ (figure 4) and $k_{relax} = 10^5$, 10^6 or 10^7 s⁻¹ (figure 5).

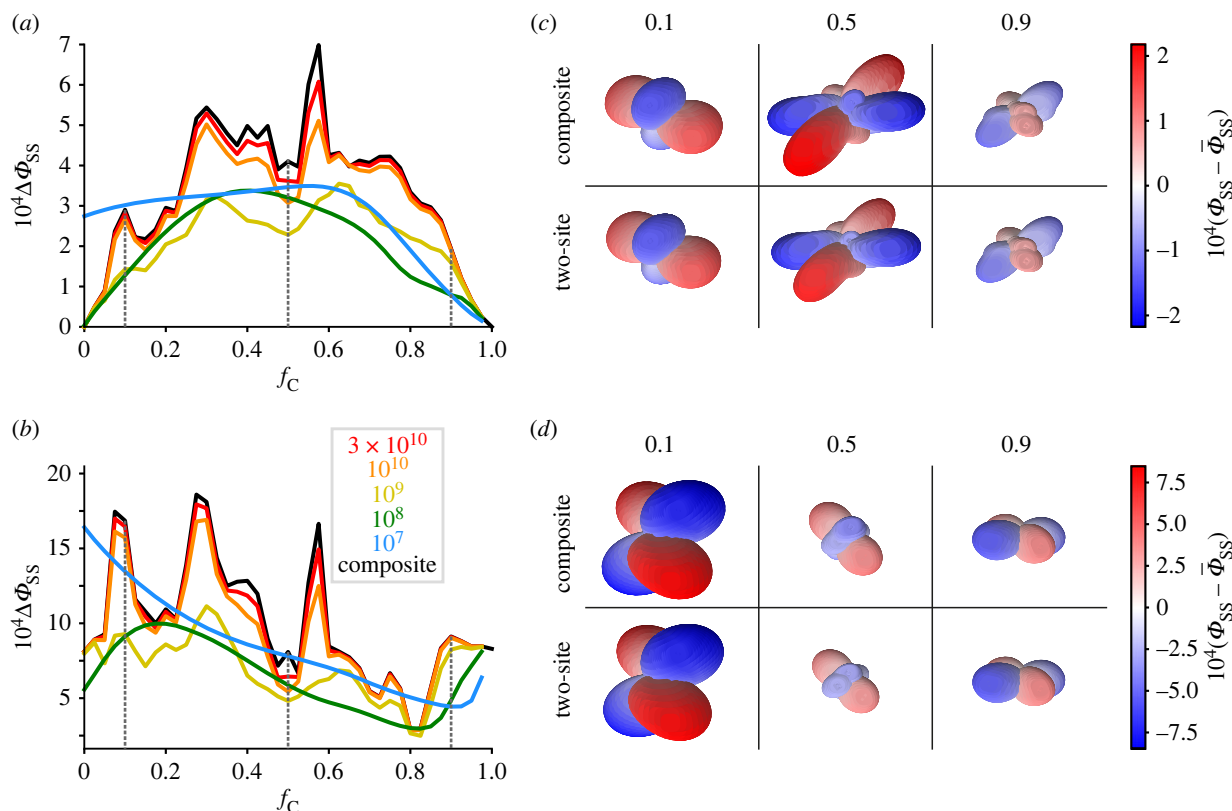


Figure 4. Comparisons of the anisotropy of the SS quantum yield, $\Delta\Phi_{SS}$, for the two-site and composite radical pair models. (a,b) dependence of $\Delta\Phi_{SS}$ on f_C with k_{CD} values in s^{-1} as indicated. (c,d) Anisotropy surface plots for $f_C = 0.1, 0.5$ and 0.9 (corresponding to the vertical dashed lines in (a) and (b)) for the composite and two-site models with $k_{CD} = 3 \times 10^{10} s^{-1}$. (a,c) $k_{Cr} = k_{Dr} = 10^6 s^{-1}$, $k_{Dr} = k_{Cr} = 0$. (b,d) $k_{Cr} = 1.2 \times 10^7 s^{-1}$, $k_{Dr} = 3.4 \times 10^5 s^{-1}$, $k_{Cr} = k_{Dr} = 10^6 s^{-1}$. The spin-relaxation rate was $k_{relax} = 10^6 s^{-1}$ in all cases. In (a) and (b) the black trace, obtained using the composite model, corresponds to the two-site model in the limit of infinitely fast electron hopping. The anisotropy surface plots (c) and (d) were obtained by calculating $\Phi_{SS}(\Omega)$ for 1601 spherically distributed magnetic field directions, Ω . The distance from the centre of the plot to the surface in a direction Ω is proportional to the difference between $\Phi_{SS}(\Omega)$ and the spherical average, $\bar{\Phi}_{SS}$. Red and blue indicate magnetic field directions in which $\Phi_{SS}(\Omega)$ is larger and smaller, respectively, than $\bar{\Phi}_{SS}$. See electronic supplementary material, section S3 for additional anisotropy surface plots.

Values of $k_{relax} \approx 10^6 s^{-1}$ allow time for electron Larmor precession (frequency = 1.4 MHz in a 50 μT field) to affect the spin dynamics before the spin coherence is irreversibly lost.

If $RP1_C$ and $RP1_D$ interconvert sufficiently rapidly, we anticipate that they can be treated as a single ‘composite’ radical pair described by figure 2a with a single stochastic Liouville equation (see electronic supplementary material, section S1 for details). The hyperfine and dipolar interactions of this composite species are averages, weighted by the fractional equilibrium populations of $RP1_C$ and $RP1_D$:

$$f_C = \frac{k_{DC}}{k_{CD} + k_{DC}} \text{ and } f_D = \frac{k_{CD}}{k_{CD} + k_{DC}}. \quad (3.2)$$

Weighted-average rate constants were obtained similarly:

$$\langle k_r \rangle = f_C k_{Cr} + f_D k_{Dr} \text{ and } \langle k_f \rangle = f_C k_{Cf} + f_D k_{Df}. \quad (3.3)$$

Hyperfine tensors, calculated by density functional methods [47], were rotated to match the relative orientations of FAD, Trp_C and Trp_D in the crystal structure of *CiCry4a* [37,48]. As the computational resources required for the simulations scale steeply with the number of spins, only a subset of the hyperfine interactions in the flavin and tryptophan radicals could be included. From among the nuclei with the largest anisotropic hyperfine interactions, three were selected (see electronic supplementary material, figure S1 for atom labelling schemes): N5 in $FAD^{\bullet-}$ (FN5) and N1 and H1 in each of $Trp_C H^{\bullet+}$ and $Trp_D H^{\bullet+}$ (WN1, WH1). FN5 and WN1 were used for the calculations shown in figure 4. All three nuclear spins were used for figure 5. The Liouvillian matrices for the two-site and composite models

had dimensions $32Z^2$ and $16Z^2$, respectively, where $Z = 27$ or 108 for the two- and three nuclei calculations, respectively.

4. Results

We start by comparing the two-site $RP1_C \leftrightarrow RP1_D$ approach (figure 2b) with the composite model (figure 2a) in which the two rapidly interconverting radical pairs act as a single entity with weighted-average properties. Figure 4 shows the dependence of the reaction yield anisotropy, $\Delta\Phi_{SS}$, on the rate constants (k_{CD} and k_{DC}) for interconversion of $RP1_C$ and $RP1_D$ for two sets of recombination and forward reaction rate constants (k_{Cr} , k_{Cf} , k_{Dr} and k_{Df}). The first set, used for figure 4a,c, corresponds to the extreme case in which recombination is exclusively from $RP1_C$ and the forward reaction is exclusively that of $RP1_D$: $k_{Cr} = k_{Df} = 1.0 \times 10^6 s^{-1}$, $k_{Dr} = k_{Cf} = 0$. In the second set, used for figure 4b,d, $k_{Cr} = 1.2 \times 10^7 s^{-1}$ and $k_{Dr} = 3.4 \times 10^5 s^{-1}$ (estimates from Xu *et al.* [39]) and $k_{Cf} = k_{Df} = 1.0 \times 10^6 s^{-1}$. For both sets, the $1.0 \times 10^6 s^{-1}$ values were chosen (i) to allow time for the 50 μT magnetic field to significantly affect the spin dynamics and (ii) so that the forward reaction can compete with recombination.

In figure 4a,b, $\Delta\Phi_{SS}$ is plotted (in colour) as a function of f_C , the fraction of radical pairs in the $RP1_C$ state, for five values of k_{CD} , with k_{DC} given by $f_C k_{CD} / (1 - f_C)$ (equation (3.2)). Also shown are the equivalent calculations for the composite radical pair (in black). As anticipated, the

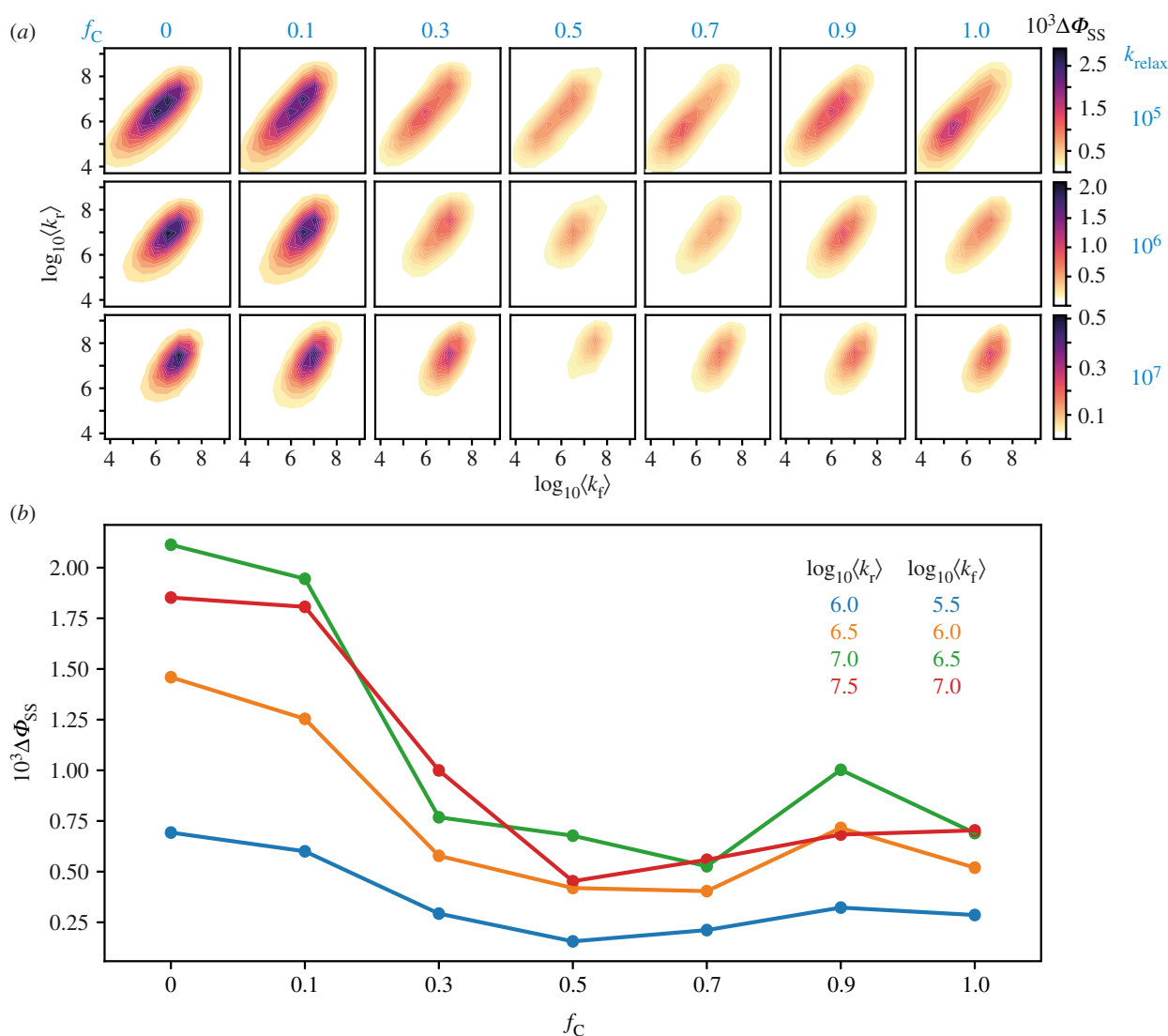


Figure 5. (a) Dependence of $\Delta\Phi_{SS}$ on $\log_{10}\langle k_r \rangle$ and $\log_{10}\langle k_f \rangle$, calculated using the composite model for seven values of f_C (columns) and three values of k_{relax} (10^5 , 10^6 , 10^7 s $^{-1}$, rows). The nuclear spins included in the calculation were FN5, WN1 and WH1. (b) Variation of $\Delta\Phi_{SS}$ with f_C for four combinations of $\langle k_r \rangle$ and $\langle k_f \rangle$, with $k_{relax} = 10^6$ s $^{-1}$. The data shown in (b) were taken from the middle row of (a). The values of $\langle k_r \rangle$ and $\langle k_f \rangle$ for (b) were chosen to satisfy the condition for $\Delta\Phi_{SS}$ to be large, i.e. $\langle k_r \rangle \approx 3\langle k_f \rangle$ and 3×10^5 s $^{-1} \leq k_f \leq 10^7$ s $^{-1}$.

correspondence between the two-site and composite models improves as k_{CD} and k_{DC} are increased, with respectable, albeit not perfect, agreement when $k_{CD} > 10^{10}$ s $^{-1}$, a condition satisfied by the k_{CD} and k_{DC} values estimated by Xu *et al.*: $(1.3 \pm 0.4) \times 10^{10}$ s $^{-1}$ and $(1.5 \pm 0.4) \times 10^{10}$ s $^{-1}$, respectively. The similarity of the predictions of the two models can also be seen from the three-dimensional representations of the anisotropic component of Φ_{SS} shown in figure 4c,d for three values of f_C with $k_{CD} = 3 \times 10^{10}$ s $^{-1}$. Although the calculations shown in figure 4 included only two hyperfine interactions (FN5 and WN1), there is no reason to think that the composite model would be significantly less valid for radical pairs with a more realistic number of nuclear spins (see electronic supplementary material, section S1.4 for details).

Figure 4 confirms that if the $RP1_C \leftrightarrow RP1_D$ interchange is fast enough, the composite model provides a reliable picture of the overall magnetic sensitivity of the system. This is a considerable simplification both conceptually and computationally and has allowed figure 5 to be calculated with three instead of two nuclear spins. This difference explains the less structured appearance of figure 5b compared to figure 4a,b (see electronic supplementary material, section S4).

With its validity confirmed, the composite model was then used to explore the dependence of the signal on the different degrees of freedom available to the system: the reaction rate constants, the spin-relaxation rate and the position of the equilibrium. Figure 5a shows contour plots of $\Delta\Phi_{SS}$ calculated for weighted-average rate constants $\langle k_r \rangle$ and $\langle k_f \rangle$ in the range 10^4 – 10^9 s $^{-1}$ (y- and x-axes, respectively; see electronic supplementary material, table S4) for seven values of f_C and three spin-relaxation rate constants. Note that these data are not presented in the same way as in figure 4 in which specific values of k_{CD} , k_{CD} , k_{Dr} and k_{Df} were used. By plotting $\Delta\Phi_{SS}$ as a function of $\langle k_r \rangle$ and $\langle k_f \rangle$ in figure 5, two contour plots with the same value of k_{relax} (i.e. in the same row) and different values of f_C only differ in the weighted-average parameters of the $\text{TrpH}^{\bullet+}$ hyperfine and $\text{FAD}^{\bullet-}$ – $\text{TrpH}^{\bullet+}$ dipolar interactions.

Within each contour plot, the maximum signal occurs for values of $\langle k_r \rangle$ and $\langle k_f \rangle$ near the centre of the 10^4 – 10^9 s $^{-1}$ range, with $\langle k_r \rangle \approx 3\langle k_f \rangle$. This can be rationalized as follows [49]. If the recombination and forward reactions are too slow, the magnetic field effects are attenuated by spin relaxation. If they are too fast, there is insufficient time for the 50 μT magnetic field to affect the spin dynamics. If $\langle k_r \rangle$ and $\langle k_f \rangle$

are too different, the competition between the two reactions is ineffective.

Each column in figure 5a shows the effect of spin relaxation for a given value of f_C . When the spins relax more rapidly, the signal strength drops and its maximum occurs for larger values of $\langle k_r \rangle$ and $\langle k_f \rangle$. The variations along the rows of figure 5a reflect the changes in the average dipolar and hyperfine interactions for different proportions of $RP1_C$ and $RP1_D$. Generally speaking, the signal is largest when $0.0 \leq f_C \leq 0.1$ and drops as f_C increases. These variations can be seen more clearly in figure 5b for selected values of $\langle k_r \rangle$ and $\langle k_f \rangle$. They appear to result mainly from the dependence of the mean dipolar interaction on f_C : the larger the dipolar interaction, the more it inhibits the singlet-triplet mixing caused by the magnetic field [44] (electronic supplementary material, section S4.3). Using centre-to-centre distances from $FAD^{\bullet-}$ to the two $TrpH^{\bullet+}$ radicals (electronic supplementary material, table S1), the average dipolar interaction rises from $\langle D \rangle = -8.1$ MHz ($f_C = 0$) to -14.3 MHz ($f_C = 1$).

The overall conclusion that can be drawn from figure 5 is that if there are no constraints on the values of the averaged rate constants $\langle k_r \rangle$ and $\langle k_f \rangle$, the largest signal available from the composite radical pair should occur for $0.0 \leq f_C \leq 0.1$, i.e. $\geq 90\%$ $RP1_D$ rapidly interconverting with $\leq 10\%$ $RP1_C$.

5. Discussion

Three main conclusions come from the simulations presented in figures 4 and 5. (i) Provided their interconversion is fast enough (k_{CD} and $k_{DC} > 10^{10} \text{ s}^{-1}$), the third ($RP1_C$) and fourth ($RP1_D$) radical pairs formed by sequential electron transfers along the Trp-tetrad in *ErCry4a* should behave as a single entity with weighted-average magnetic and kinetic properties (figure 4). (ii) If there are no restrictions on the values of the mean rate constants, $\langle k_r \rangle$ and $\langle k_f \rangle$, the largest anisotropic signals ($\Delta\Phi_{SS}$) can be expected when the equilibrium proportion of $RP1_D$ is 90–100% (i.e. $f_C = 0.0$ – 0.1 , figure 5). (iii) The largest values of $\Delta\Phi_{SS}$ (figure 5a) occur when $\langle k_r \rangle \approx 3\langle k_f \rangle$ and $\langle k_f \rangle \approx 2 \times 10^6 \text{ s}^{-1}$ (when $k_{\text{relax}} = 10^5 \text{ s}^{-1}$), $\langle k_f \rangle \approx 6 \times 10^6 \text{ s}^{-1}$ (when $k_{\text{relax}} = 10^6 \text{ s}^{-1}$) and $\langle k_f \rangle \approx 9 \times 10^6 \text{ s}^{-1}$ (when $k_{\text{relax}} = 10^7 \text{ s}^{-1}$).

The immediate question raised by (ii) and (iii) is whether the values of $\langle k_r \rangle$ and $\langle k_f \rangle$ required to achieve large $\Delta\Phi_{SS}$ are (i) realistic and (ii) compatible with small values of f_C . The answer depends on the rate of spin relaxation (with which we start the discussion below). Before doing so, we note that Xu *et al.* [39] determined the strength of the dipolar interaction, D , in the $FAD^{\bullet-}$ – $TrpH^{\bullet+}$ radical pair formed photochemically in WT *ErCry4a* and hence the centre-to-centre separation of the radicals. Based on the crystal structure of the highly homologous pigeon protein, *ClCry4a* [37], the difference between the values of $\langle D \rangle$ expected for $f_C = 0.0$ and $f_C = 0.1$ was within the experimental error in the measurement of D . These experiments are, therefore, consistent with a small fraction of $RP1_C$ ($f_C \leq 0.1$) in rapid exchange with $RP1_D$.

5.1. Spin-relaxation rates

As described in §3, there being no experimental measurements of spin-relaxation rates of radicals in Crys, the best estimates of k_{relax} come from molecular dynamics simulations combined with Bloch–Redfield relaxation theory which suggest values

in excess of 10^6 s^{-1} [45]. For the electrons to relax as slowly as 10^5 s^{-1} the protein would either have to be almost rigid or the radicals within it would have to undergo very rapid, very low amplitude librational and torsional motions. Neither extreme is plausible.

A number of authors have used relaxation rates much slower than 10^6 s^{-1} in computer simulations of magnetic field effects purporting to be relevant to magnetoreception. More commonly spin relaxation has been completely ignored. In our view, it is unrealistic to assume, in effect, that flavin and tryptophan radicals in a large protein behave in the same way as small radicals undergoing picosecond rotational diffusion in a non-viscous solvent, the only situation in which one could expect relaxation rates slower than about 10^6 s^{-1} at physiological temperatures.

To summarize, the discussion below is based on the premise that $k_{\text{relax}} \geq 10^6 \text{ s}^{-1}$. This implies (figure 5a) that $\langle k_r \rangle$ and $\langle k_f \rangle$ must lie in the approximate range 10^6 – 10^8 s^{-1} .

5.2. Recombination rates

We look first at the case of $f_C = 0$ in which $RP1_D$ is solely responsible for the magnetic field effects. In this limit, the condition that $\langle k_r \rangle \approx \langle k_f \rangle \geq 10^6 \text{ s}^{-1}$ is simply $k_{Dr} \approx k_{Df} \geq 10^6 \text{ s}^{-1}$. A rough upper limit on the rate constant for direct back electron transfer from $FAD^{\bullet-}$ to $TrpD^{\bullet+}$ (in s^{-1}), assuming zero activation energy, can be obtained from [50]:

$$\log_{10} k_r \leq 13 - 0.6 (R - 3.6) \quad (5.1)$$

where R (in Å) is the edge-to-edge separation of the electron donor and acceptor. With $R = 16.8$ Å for $RP1_D$ (electronic supplementary material, table S1), equation (5.1) gives $k_{Dr} \leq 1.1 \times 10^5 \text{ s}^{-1}$. Using $R = 16.0$ Å and an approximate activation energy, Xu *et al.* [39] obtained a similar estimate: $k_{Dr} \approx (3.4 \pm 1.5) \times 10^5 \text{ s}^{-1}$. Such small values of $\langle k_r \rangle$ are not compatible with a large $\Delta\Phi_{SS}$ when $k_{\text{relax}} \geq 10^6 \text{ s}^{-1}$. It is, therefore, difficult to see how $RP1_D$ acting alone in *ErCry4a* could form the basis of a sensitive magnetic compass. Müller *et al.* [51] reached the same conclusion based on measurements of electron transfer rates in *Xenopus laevis* (6–4) photolyase which also has a Trp-tetrad.

We now look at $f_C = 0.1$ to see whether a 1 : 9 combination of $RP1_C$ and $RP1_D$ in rapid equilibrium (figure 5) could make for a more satisfactory sensor. Applying equation (5.1) to $RP1_C$, with an edge-to-edge separation of 13.6 Å (electronic supplementary material, table S1), one obtains an approximate upper limit on k_{Cr} of $1.1 \times 10^7 \text{ s}^{-1}$. Xu *et al.* [39] arrived at the same number, $k_{Cr} \approx (1.2 \pm 0.5) \times 10^7 \text{ s}^{-1}$, using the slightly smaller separation of 13.3 Å and by including an activation energy term in equation (5.1). Combining $k_{Cr} = 1.2 \times 10^7 \text{ s}^{-1}$ with $k_{Dr} = 1.1 \times 10^5 \text{ s}^{-1}$ (from above) gives $\langle k_r \rangle = 0.1k_{Cr} + 0.9k_{Dr} \approx 1.3 \times 10^6 \text{ s}^{-1}$ which satisfies one of the conditions for $\Delta\Phi_{ss}$ to be relatively large, namely $\langle k_r \rangle \geq 10^6 \text{ s}^{-1}$.

5.3. Tryptophan deprotonation rates

For a composite radical pair with $\langle k_r \rangle \approx 1.3 \times 10^6 \text{ s}^{-1}$ and $f_C = 0.1$, to give a large value of $\Delta\Phi_{SS}$, the mean rate constant for the forward reaction, $\langle k_f \rangle$, would (using the $\langle k_r \rangle \approx 3\langle k_f \rangle$ condition) need to be $\approx 4.3 \times 10^5 \text{ s}^{-1}$. This reaction, in which the $TrpH^{\bullet+}$ radicals are stabilized by loss of the indole proton (WH1) to form neutral Trp^{\bullet} radicals, has been studied

for several members of the Cry-photolyase superfamily. Deprotonation time constants span four orders of magnitude, from 100–400 ps [52–54], to 200–400 ns [51,55–58], to 1–4 μ s [41,51,59,60]. The very short, sub-nanosecond, lifetimes are for proteins that have an internal H^+ acceptor and/or water molecules close to the indole nitrogen atom [52–54]; there is no evidence for either feature in the crystal structure of *Cl*Cry4a or in the molecular dynamics simulations of *Er*Cry4a for either $Trp_C H^{++}$ or $Trp_D H^{++}$ [39]. Slower deprotonation (greater than 100 ns) occurs when the solvent acts as the H^+ acceptor. In only two cases have deprotonation rates been measured for $Trp_C H^{++}$ and $Trp_D H^{++}$ in the same protein (the former by replacing Trp_D by phenylalanine). Müller *et al.* [51] found time constants of 400 ns for $Trp_C H^{++}$ and 2.5 μ s for $Trp_D H^{++}$ in *X. laevis* (6–4) photolyase, while Xu *et al.* [39] reported a 100 ns component in the decays of both $RP1_C$ and $RP1_D$ in *Er*Cry4a. The latter was interpreted in terms of a composite radical pair with $\langle k_{Cr} \rangle \approx \langle k_{Dr} \rangle \approx (5–10) \times 10^6 \text{ s}^{-1}$.

While most of these measurements on purified proteins are inconsistent with $\langle k_f \rangle \approx 4.3 \times 10^5 \text{ s}^{-1}$, there is no reason why release of the indole proton from either $Trp_C H^{++}$ or $Trp_D H^{++}$ *in vivo* necessarily occurs at the same rate as for the purified protein. Interactions of Crys with other proteins, required either for molecular alignment or signal transduction [42,61], could reduce the solvent accessibility and hence the deprotonation rate. Additionally, reasonably large values of $\Delta\Phi_{SS}$ can still be expected (figure 5a) even though the optimum condition, $\langle k_r \rangle = 3\langle k_f \rangle$, may not be satisfied exactly. In summary, it seems possible that $\langle k_f \rangle$, like $\langle k_r \rangle$, could, *in vivo*, fall in the range required for a large $\Delta\Phi_{SS}$.

5.4. Tyr319 reduction

Potentially, there is an alternative reaction pathway from the composite radical pair to the SS. Tyr319 (figure 1) has an edge-to-edge distance to Trp_D of 3.9 Å (electronic supplementary material, table S1), and appears well placed to be oxidized by $Trp_D H^{++}$. In several members of the photolyase-Cry superfamily there is a tyrosine at the far end of the Trp-triad that donates an electron to the terminal $Trp_C H^{++}$ radical, thus extending the electron transfer chain and stabilizing the $FAD^{\bullet-}$ radical against back electron transfer [40,53,54,62–66]. The tyrosine radical ($TyrO^{\bullet}$) so formed is solvent-exposed and therefore able to be reduced by exogenous electron donors, potentially allowing the efficient formation of a SS containing $FADH^{\bullet}$ as the only radical.

If Tyr319 oxidation rather than $Trp_{C,D} H^{++}$ deprotonation is the major pathway to the SS, the reaction scheme in figure 2b changes to that shown in figure 6. Recombination may be taken to occur exclusively from $RP1_C$ (smaller donor–acceptor separation than $RP1_D$), while the SS is formed from $RP1_D$ via spin-independent electron transfer from Tyr319 to $Trp_D H^{++}$. Reduction of $Trp_C H^{++}$ by Tyr319 is likely to be an order of magnitude slower given the approximately 3 Å larger donor–acceptor distance. Recombination of both $RP1_D$ and $[FAD^{\bullet-} TyrO^{\bullet}]$ to the GS is assumed to be negligibly slow due to the large edge-to-edge distances, 16.8 and 20.3 Å, respectively (electronic supplementary material, table S1).

The conditions required for this modified reaction scheme (figure 6) to deliver large values of $\Delta\Phi_{SS}$ are exactly the same as for the reactions in figure 2b, namely $10^6 \text{ s}^{-1} < \langle k_r \rangle \approx 3\langle k_f \rangle < 10^8 \text{ s}^{-1}$ where the subscript in $\langle k_f \rangle$ now refers to electron transfer

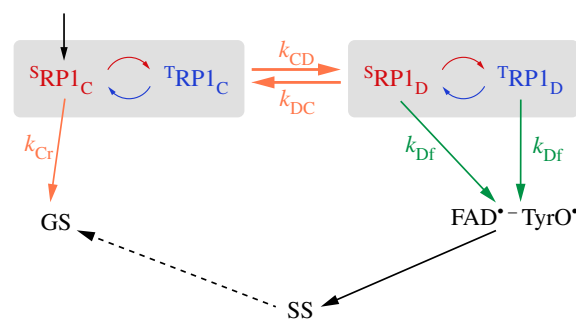


Figure 6. Modified version of figure 2b in which the major route to the SS is via reduction of $Trp_D H^{++}$ by Tyr319 instead of deprotonation of $Trp_C H^{++}$ and $Trp_D H^{++}$. Contrary to a recent speculation [38], the edge-to-edge separation of $FAD^{\bullet-}$ and $TyrO^{\bullet}$ (20.3 Å, electronic supplementary material, table S1) is such that this radical pair is even less likely than $RP1_D$ to recombine rapidly enough to give a significant magnetic field effect.

from Tyr319 to $Trp_D H^{++}$. If, as assumed in figure 6, $k_{Cr} \gg k_{Dr}$ and $k_{Cr} \ll k_{Dr}$, then $\langle k_r \rangle \approx f_C k_{Cr}$ and $\langle k_f \rangle \approx (1 - f_C) k_{Dr}$. As long as k_{Dr} is in the approximate range 10^6 – 10^8 s^{-1} , the scheme in figure 6 could be just as suitable as that in figure 2b for efficient magnetic compass sensing.

There is some evidence that Tyr319 does indeed donate an electron to $Trp_D H^{++}$ in avian Cry4a. Otsuka *et al.* [38] have reported long-lived $TyrO^{\bullet}$ radicals in chicken (*Gallus gallus*) Cry4a while Zoltowski *et al.* [37] found that mutating Tyr319 to aspartic acid in *Cl*Cry4a decreased the quantum yield of FAD photoreduction and modified the photoreduction kinetics. Xu *et al.* [39], however, did not detect light-induced $TyrO^{\bullet}$ radicals in robin Cry4a either by transient absorption or electron paramagnetic resonance, although a possible explanation in the former case is that the UV–visible absorption band of $TyrO^{\bullet}$ is narrow and heavily overlapped by the bands of the various FAD and Trp species. Nevertheless, it seems possible that Tyr319 could be the terminal electron donor in *Er*Cry4a *in vivo* where the rate of electron transfer to $Trp_D H^{++}$ might be tuned by protein–protein interactions with signalling partners. If so, then reduction of $Trp_D H^{++}$ by Tyr319 could, in conjunction with spin-selective recombination of $RP1_C$, give rise to a significant $\Delta\Phi_{SS}$.

An interesting feature of the scheme in figure 6 is that the two rate constants $\langle k_r \rangle = f_C k_{Cr}$ and $\langle k_f \rangle = (1 - f_C) k_{Dr}$ depend on the properties of different tryptophan radicals (C and D, respectively), providing scope for independent optimization of $\langle k_r \rangle$ and $\langle k_f \rangle$. Amino acid mutations in the neighbourhood of $Trp_C H^{++}$, for example, could tune $\langle k_r \rangle$ without affecting $\langle k_f \rangle$, and *vice versa*. This situation could also occur for the scheme in figure 2b if $k_{Cr} \ll k_{Dr}$ and $k_{Cr} \gg k_{Dr}$ (see electronic supplementary material, section S2). By contrast, if only one radical pair is involved (figure 2a), a mutation that led to a favourable change in k_r might well have the opposite effect on k_f .

6. Conclusion

By means of spin dynamics simulations, we have explored the potential advantages of simultaneously involving the third and fourth sequentially formed flavin–tryptophan radical pairs in magnetic sensing and signalling in avian Cry4a. A composite radical pair with weighted-average properties of its two components, could, at least in theory, offer ‘the best of

both worlds'. That is, the stronger magnetic sensitivity afforded by $[\text{FAD}^{\bullet-} \text{Trp}_\text{C}\text{H}^{\bullet+}]$ and the superior potential of $[\text{FAD}^{\bullet-} \text{Trp}_\text{D}\text{H}^{\bullet+}]$ to form a SS via oxidation of Tyr319 (figure 6). Plants, whose Crys contain only three tryptophans, have no known biological requirement to respond to the direction of the Earth's magnetic field, and so might not need to separate the magnetic sensing and signalling functions in the same way as a migratory bird. The Cry from *Drosophila melanogaster* has four tryptophans, like avian Cry4a, but lacks the terminal tyrosine. This could be relevant if the various magnetic behaviours reported for fruit flies turn out to offer no biological advantage to these non-migratory animals [67–75].

Clearly, experiments are needed to test this idea. One possibility would be to mutate amino acid residues in the neighbourhood of the two tryptophans in such a way as to shift the position of the putative equilibrium. For example, introducing a negative charge or removing a positive charge in the vicinity of Trp_C could be expected to stabilize $[\text{FAD}^{\bullet-} \text{Trp}_\text{C}\text{H}^{\bullet+}]$ and so change the magnetic sensitivity. Another option would be to seek conditions for the *in vitro* experiments that more closely resemble those *in vivo*. For example, it could be that electron transfer from Tyr319 to the fourth tryptophan radical is favoured by protein–protein interactions and could be revealed by studying Cry4a in association with one of the potential signalling partners identified by Wu *et al.* [42] Thus, it may be possible to get

further insight into whether four tryptophans (or four tryptophans and a tyrosine) are better than three.

Data accessibility. The data are provided in the electronic supplementary material [76].

Authors' contributions. S.Y.W. and Y.W. performed the spin dynamics simulations. S.Y.W. calculated the solvent accessibilities with assistance from I.A.S. All authors discussed the results. Y.W., H.M. and I.A.S. commented on the manuscript which was written by S.Y.W. and P.J.H.

Competing interests. The authors declare no competing interests.

Funding. We acknowledge the financial support of the Deutsche Forschungsgemeinschaft, project nos. 395940726 (SFB 1372, Magnetoreception and Navigation in Vertebrates) and GRK1885 and the European Research Council (under the European Union's Horizon 2020 research and innovation programme, grant agreement no. 810002, Synergy Grant, QuantumBirds). I.A.S. thanks the Lundbeck Foundation, the Volkswagen Foundation (Lichtenberg Professorship) and the Ministry for Science and Culture of Lower Saxony ('Simulations meet experiments on the nanoscale: opening up the quantum world to artificial intelligence', SMART). Computational resources for the simulations were provided by the DeIC National HPC Center, SDU and the CARL Cluster at the Carl-von-Ossietzky University of Oldenburg, which is supported by the DFG under INST grant no. 184/157-1 FUGG and the Ministry of Science and Culture (MWK) of the Lower Saxony State. The work was also supported by the North German Supercomputing Alliance (HLRN).

Acknowledgements. We are grateful to Stuart Mackenzie and Christiane Timmel for detailed comments on the manuscript and to Maja Hanić for assistance with the solvent accessibility calculations.

References

1. Wiltschko R, Wiltschko W. 1995 *Magnetic orientation in animals*. Berlin, Germany: Springer.
2. Mouritsen H. 2018 Long-distance navigation and magnetoreception in migratory animals. *Nature* **558**, 50–59. (doi:10.1038/s41586-018-0176-1)
3. Schulten K, Swenberg CE, Weller A. 1978 A biomagnetic sensory mechanism based on magnetic field modulated coherent electron spin motion. *Z. Phys. Chem* **111**, 1–5. (doi:10.1524/zpch.1978.111.1.001)
4. Ritz T, Adem S, Schulten K. 2000 A model for photoreceptor-based magnetoreception in birds. *Biophys. J.* **78**, 707–718. (doi:10.1016/S0006-3495(00)76629-X)
5. Hore PJ, Mouritsen H. 2016 The radical pair mechanism of magnetoreception. *Annu. Rev. Biophys.* **45**, 299–344. (doi:10.1146/annurev-biophys-032116-094545)
6. Karki N, Vergis S, Zoltowski BD. 2021 Cryptochromes: photochemical and structural insight into magnetoreception. *Protein Sci.* **30**, 1521–1534. (doi:10.1002/pro.4124)
7. Wiltschko R, Niessner C, Wiltschko W. 2021 The magnetic compass of birds: the role of cryptochrome. *Front. Physiol.* **12**, 667000. (doi:10.3389/fphys.2021.667000)
8. Wong SY, Frederiksen A, Hanic M, Schuhmann F, Grüning G, Hore PJ, Solovov IA. 2021 Navigation of migratory songbirds: a quantum magnetic compass sensor. *Neuroforum* (doi:10.1515/nf-2021-0005)
9. Wiltschko W, Wiltschko R. 1972 Magnetic compass of European robins. *Science* **176**, 62–64. (doi:10.1126/science.176.4030.62)
10. Wiltschko R, Stappert K, Thalau P, Wiltschko W. 2010 Directional orientation of birds by the magnetic field under different light conditions. *J. R. Soc. Interface* **7**, S163–S177. (doi:10.1098/rsif.2009.0367.focus)
11. Zapka M, Heyers D, Liedvogel M, Jarvis ED, Mouritsen H. 2010 Night-time neuronal activation of cluster N in a day- and night-migrating songbird. *Eur. J. Neurosci.* **32**, 619–624. (doi:10.1111/j.1460-9568.2010.07311.x)
12. Zapka M *et al.* 2009 Visual but not trigeminal mediation of magnetic compass information in a migratory bird. *Nature* **461**, 1274–1278. (doi:10.1038/nature08528)
13. Chaves I *et al.* 2011 The cryptochromes: blue light photoreceptors in plants and animals. *Annu. Rev. Plant Biol.* **62**, 335–364. (doi:10.1146/annurev-arplant-042110-103759)
14. Liedvogel M, Mouritsen H. 2010 Cryptochromes—a potential magnetoreceptor: what do we know and what do we want to know? *J. R. Soc. Interface* **7**, S147–S162. (doi:10.1098/rsif.2009.0411.focus)
15. Wang Q, Lin C. 2020 Mechanisms of cryptochrome-mediated photoreponses in plants. *Annu. Rev. Plant Biol.* **71**, 103–129. (doi:10.1146/annurev-arplant-050718-100300)
16. Möller A, Sagasser S, Wiltschko W, Schierwater B. 2004 Retinal cryptochrome in a migratory passerine bird: a possible transducer for the avian magnetic compass. *Naturwissenschaften* **91**, 585–588. (doi:10.1007/s00114-004-0578-9)
17. Mouritsen H, Janssen-Bienhold U, Liedvogel M, Feenders G, Stalleicken J, Dirks P, Weiler R. 2004 Cryptochromes and neuronal-activity markers colocalize in the retina of migratory birds during magnetic orientation. *Proc. Natl Acad. Sci. USA* **101**, 14 294–14 299. (doi:10.1073/pnas.0405968101)
18. Niessner C, Denzau S, Gross JC, Peichl L, Bischof HJ, Fleissner G, Wiltschko W, Wiltschko R. 2011 Avian ultraviolet/violet cones identified as probable magnetoreceptors. *PLoS ONE* **6**, e20091. (doi:10.1371/journal.pone.0020091)
19. Bolte P *et al.* 2016 Localisation of the putative magnetoreceptive protein cryptochrome 1b in the retinas of migratory birds and homing pigeons. *PLoS ONE* **11**, e0147819. (doi:10.1371/journal.pone.0147819)
20. Niessner C, Gross JC, Denzau S, Peichl L, Fleissner G, Wiltschko W, Wiltschko R. 2016 Seasonally changing cryptochrome 1b expression in the retinal ganglion cells of a migrating passerine bird. *PLoS ONE* **11**, e0150377. (doi:10.1371/journal.pone.0150377)
21. Günther A, Einwich A, Sjulstok E, Feederle R, Bolte P, Koch KW, Solovov IA, Mouritsen H. 2018 Double-cone localization and seasonal expression pattern suggest a role in magnetoreception for European robin cryptochrome 4. *Curr. Biol.* **28**, 211–223. (doi:10.1016/j.cub.2017.12.003)

22. Einwich A, Dedek K, Seth PK, Laubinger S, Mouritsen H. 2020 A novel isoform of cryptochrome 4 (Cry4b) is expressed in the retina of a night-migratory songbird. *Sci. Rep.* **10**, 15794.
23. Hochstoege T *et al.* 2020 The biophysical, molecular, and anatomical landscape of pigeon CRY4: a candidate light-based quantum magnetosensor. *Sci. Adv.* **6**, eabb9110. (doi:10.1126/sciadv.abb9110)
24. Bolte P *et al.* 2021 Cryptochrome 1a localisation in light- and dark-adapted retinas of several migratory and non-migratory bird species: no signs of light-dependent activation. *Ethol. Ecol. Evol.* **33**, 248–272. (doi:10.1080/03949370.03942020.01870571)
25. Pinzon-Rodriguez A, Muheim R. 2021 Cryptochrome expression in avian UV cones: revisiting the role of CRY1 as magnetoreceptor. *Sci. Rep.* **11**, 12683. (doi:10.1038/s41598-021-92056-8)
26. Player TC, Hore PJ. 2019 Viability of superoxide-containing radical pairs as magnetoreceptors. *J. Chem. Phys.* **151**, 225101. (doi:10.1063/1.5129608)
27. Hogben HJ, Efimova O, Wagner-Rundell N, Timmel CR, Hore PJ. 2009 Possible involvement of superoxide and dioxygen with cryptochrome in avian magnetoreception: origin of Zeeman resonances observed by *in vivo* EPR spectroscopy. *Chem. Phys. Lett.* **480**, 118–122. (doi:10.1016/j.cplett.2009.08.051)
28. Pooam M, Arthaut LD, Burdick D, Link J, Martino CF, Ahmad M. 2019 Magnetic sensitivity mediated by the *Arabidopsis* blue-light receptor cryptochrome occurs during flavin reoxidation in the dark. *Planta* **249**, 319–332. (doi:10.1007/s00425-018-3002-y)
29. Niessner C, Denzau S, Peichl L, Wiltchko W, Wiltchko R. 2014 Magnetoreception in birds: I. Immunohistochemical studies concerning the cryptochrome cycle. *J. Exp. Biol.* **217**, 4221–4224. (doi:10.1242/jeb.110965)
30. Wiltchko R, Ahmad M, Niessner C, Gehring D, Wiltchko W. 2016 Light-dependent magnetoreception in birds: the crucial step occurs in the dark. *J. R. Soc. Interface* **13**, 20151010. (doi:10.1098/rsif.2015.1010)
31. Niessner C, Denzau S, Peichl L, Wiltchko W, Wiltchko R. 2018 Magnetoreception: activation of avian cryptochrome 1a in various light conditions. *J. Comp. Physiol. A* **204**, 977–984. (doi:10.1007/s00359-018-1296-7)
32. Müller P, Ahmad M. 2011 Light-activated cryptochrome reacts with molecular oxygen to form a flavin-superoxide radical pair consistent with magnetoreception. *J. Biol. Chem.* **286**, 21 033–21 040. (doi:10.1074/jbc.M111.228940)
33. Kutta RJ, Archipowa N, Johannissen LO, Jones AR, Scrutton NS. 2017 Vertebrate cryptochromes are vestigial flavoproteins. *Sci. Rep.* **7**, 44906. (doi:10.1038/srep44906)
34. Ozturk N, Selby CP, Song SH, Ye R, Tan C, Kao YT, Zhong DP, Sancar A. 2009 Comparative photochemistry of animal type 1 and type 4 cryptochromes. *Biochemistry* **48**, 8585–8593. (doi:10.1021/bi901043s)
35. Mitsui H, Maeda T, Yamaguchi C, Tsuji Y, Watari R, Kubo Y, Okano K, Okano T. 2015 Overexpression in yeast, photocycle, and *in vitro* structural change of an avian putative magnetoreceptor cryptochrome 4. *Biochemistry* **54**, 1908–1917. (doi:10.1021/bi501441u)
36. Wang X, Jing C, Selby CP, Chiou Y-Y, Yang Y, Wu WJ, Sancar A, Wang J. 2018 Comparative properties and functions of type 2 and type 4 pigeon cryptochromes. *Cell. Mol. Life Sci.* **75**, 4629–4641. (doi:10.1007/s00018-018-2920-y)
37. Zoltowski BD *et al.* 2019 Chemical and structural analysis of a photoactive vertebrate cryptochrome from pigeon. *Proc. Natl Acad. Sci. USA* **116**, 19 449–19 457. (doi:10.1073/pnas.1907875116)
38. Otsuka H, Mitsui H, Miura K, Okano K, Imamoto Y, Okano T. 2020 Rapid oxidation following photoreduction in the avian cryptochrome 4 photocycle. *Biochemistry* **59**, 3615–3625. (doi:10.1021/acs.biochem.0c00495)
39. Xu J *et al.* 2021 Magnetic sensitivity of cryptochrome 4 from a migratory songbird. *Nature* **594**, 535–540. (doi:10.1038/s41586-021-03618-9)
40. Nohr D, Franz S, Rodriguez R, Paulus B, Essen L-O, Weber S, Schleicher E. 2016 Extended electron-transfer pathways in animal cryptochromes mediated by a tetrad of aromatic amino acids. *Biophys. J.* **111**, 301–311. (doi:10.1016/j.bpj.2016.06.009)
41. Maeda K *et al.* 2012 Magnetically sensitive light-induced reactions in cryptochrome are consistent with its proposed role as a magnetoreceptor. *Proc. Natl Acad. Sci. USA* **109**, 4774–4779. (doi:10.1073/pnas.1118959109)
42. Wu H, Scholten A, Einwich A, Mouritsen H, Koch KW. 2020 Protein–protein interaction of the putative magnetoreceptor cryptochrome 4 expressed in the avian retina. *Sci. Rep.* **10**, 7364. (doi:10.1038/s41598-020-64429-y)
43. Haberkorn R. 1976 Density matrix description of spin-selective radical pair reactions. *Mol. Phys.* **32**, 1491–1493. (doi:10.1080/00268977600102851)
44. Babcock NS, Kattinig DR. 2020 Electron–electron dipolar interaction poses a challenge to the radical pair mechanism of magnetoreception. *J. Phys. Chem. Lett.* **11**, 2414–2421. (doi:10.1021/acs.jpclett.0c00370)
45. Kattinig DR, Solov'yov IA, Hore PJ. 2016 Electron spin relaxation in cryptochrome-based magnetoreception. *Phys. Chem. Chem. Phys.* **18**, 12 443–12 456. (doi:10.1039/C5CP06731F)
46. Kattinig DR, Sowa JK, Solov'yov IA, Hore PJ. 2016 Electron spin relaxation can enhance the performance of a cryptochrome-based magnetic compass sensor. *New J. Phys.* **18**, 063007. (doi:10.1088/1367-2630/18/6/063007)
47. Lee AA, Lau JCS, Hogben HJ, Biskup T, Kattinig DR, Hore PJ. 2014 Alternative radical pairs for cryptochrome-based magnetoreception. *J. R. Soc. Interface* **11**, 20131063. (doi:10.1098/rsif.2013.1063)
48. Atkins C, Bajpai K, Rumball J, Kattinig DR. 2019 On the optimal relative orientation of radicals in the cryptochrome magnetic compass. *J. Chem. Phys.* **151**, 065103. (doi:10.1063/1.5115445)
49. Hore PJ. 2019 Upper bound on the biological effects of 50/60 Hz magnetic fields mediated by radical pairs. *Elife* **8**, e44179. (doi:10.7554/eLife.44179)
50. Moser CC, Anderson JLR, Dutton PL. 2010 Guidelines for tunneling in enzymes. *Biochim Biophys Acta* **1797**, 1573–1586. (doi:10.1016/j.bbabi.2010.04.441)
51. Müller P, Yamamoto J, Martin R, Iwai S, Brettel K. 2015 Discovery and functional analysis of a 4th electron-transferring tryptophan conserved exclusively in animal cryptochromes and (6–4) photolyases. *Chem. Commun.* **51**, 15 502–15 505. (doi:10.1039/C5CC06276D)
52. Immeln D, Weigel A, Kottke T, Perez Lustres JL. 2012 Primary events in the blue light sensor plant cryptochrome: intraprotein electron and proton transfer revealed by femtosecond spectroscopy. *J. Am. Chem. Soc.* **134**, 12 536–12 546. (doi:10.1021/ja302121z)
53. Muller P, Ignatz E, Kiontke S, Brettel K, Essen LO. 2018 Sub-nanosecond tryptophan radical deprotonation mediated by a protein-bound water cluster in class II DNA photolyases. *Chem. Sci.* **9**, 1200–1212. (doi:10.1039/C7SC03969G)
54. Lacombat F, Espagne A, Dozova N, Plaza P, Ignatz E, Kiontke S, Essen LO. 2018 Delocalized hole transport coupled to sub-ns tryptophanyl deprotonation promotes photoreduction of class II photolyases. *Phys. Chem. Chem. Phys.* **20**, 25 446–25 457. (doi:10.1039/C8CP04548H)
55. Aubert C, Vos MH, Mathis P, Eker APM, Brettel K. 2000 Intraprotein radical transfer during photoactivation of DNA photolyase. *Nature* **405**, 586–590. (doi:10.1038/35014644)
56. Byrdin M, Sartor V, Eker APM, Vos MH, Aubert C, Brettel K, Mathis P. 2004 Intraprotein electron transfer and proton dynamics during photoactivation of DNA photolyase from *E. coli*: review and new insights from an 'inverse' deuterium isotope effect. *Biochim. Biophys. Acta* **1655**, 64–70. (doi:10.1016/j.bbabi.2003.07.001)
57. Byrdin M, Lukacs A, Thiagarajan V, Eker AP, Brettel K, Vos MH. 2010 Quantum yield measurements of short-lived photoactivation intermediates in DNA photolyase: toward a detailed understanding of the triple tryptophan electron transfer chain. *J. Phys. Chem. A* **114**, 3207–3214. (doi:10.1021/jp9093589)
58. Muller P, Bouly JP, Hitomi K, Balland V, Getzoff ED, Ritz T, Brettel K. 2014 ATP binding turns plant cryptochrome into an efficient natural photoswitch. *Sci. Rep.* **4**, 5175. (doi:10.1038/srep05175)
59. Paulus B *et al.* 2015 Spectroscopic characterization of radicals and radical pairs in fruit fly cryptochrome-protonated and nonprotonated flavin radical-states. *FEBS J.* **282**, 3175–3189. (doi:10.1111/febs.13299)
60. Kutta RJ, Archipowa N, Scrutton NS. 2018 The sacrificial inactivation of the blue-light photosensor cryptochrome from *Drosophila melanogaster*. *Phys.*

- Chem. Chem. Phys.* **20**, 28 767–28 776. (doi:10.1039/C8CP04671A)
61. Lau JCS, Wagner-Rundell N, Rodgers CT, Green NJB, Hore PJ. 2010 Effects of disorder and motion in a radical pair magnetoreceptor. *J. R. Soc. Interface* **7**, S257–S264. (doi:10.1098/rsif.2009.0399.focus)
 62. Aubert C, Mathis P, Eker APM, Brettel K. 1999 Intraprotein electron transfer between tyrosine and tryptophan in DNA photolyase from *Anacystis nidulans*. *Proc. Natl Acad. Sci. USA* **96**, 5423–5427. (doi:10.1073/pnas.96.10.5423)
 63. Giovani B, Byrdin M, Ahmad M, Brettel K. 2003 Light-induced electron transfer in a cryptochrome blue-light photoreceptor. *Nat. Struct. Biol.* **10**, 489–490. (doi:10.1038/nsb933)
 64. Oldemeyer S, Franz S, Wenzel S, Essen LO, Mittag M, Kottke T. 2016 Essential role of an unusually long-lived tyrosyl radical in the response to red light of the animal-like cryptochrome aCRY. *J. Biol. Chem.* **291**, 14 062–14 071. (doi:10.1074/jbc.M116.726976)
 65. Oldemeyer S, Mittag M, Kottke T. 2019 Time-resolved infrared and visible spectroscopy on cryptochrome aCRY: basis for red light reception. *Biophys. J.* **117**, 490–499. (doi:10.1016/j.bpj.2019.06.027)
 66. Lacombat F, Espagne A, Dozova N, Plaza P, Muller P, Brettel K, Franz-Badur S, Essen LO. 2019 Ultrafast oxidation of a tyrosine by proton-coupled electron transfer promotes light activation of an animal-like cryptochrome. *J. Am. Chem. Soc.* **141**, 13 394–13 409. (doi:10.1021/jacs.9b03680)
 67. Gegear RJ, Casselman A, Waddell S, Reppert SM. 2008 Cryptochrome mediates light-dependent magnetosensitivity in *Drosophila*. *Nature* **454**, 1014–1018. (doi:10.1038/nature07183)
 68. Gegear RJ, Foley LE, Casselman A, Reppert SM. 2010 Animal cryptochromes mediate magnetoreception by an unconventional photochemical mechanism. *Nature* **463**, 804–807. (doi:10.1038/nature08719)
 69. Foley LE, Gegear RJ, Reppert SM. 2011 Human cryptochrome exhibits light-dependent magnetosensitivity. *Nat. Commun.* **2**, 356. (doi:10.1038/ncomms1364)
 70. Yoshii T, Ahmad M, Helfrich-Forster C. 2009 Cryptochrome mediates light-dependent magnetosensitivity of *Drosophila's* circadian clock. *PLoS Biol.* **7**, 813–819. (doi:10.1371/journal.pbio.1000086)
 71. Fedele G, Green EW, Rosato E, Kyriacou CP. 2014 An electromagnetic field disrupts negative geotaxis in *Drosophila* via a CRY-dependent pathway. *Nat. Commun.* **5**, 4391. (doi:10.1038/ncomms5391)
 72. Fedele G *et al.* 2014 Genetic analysis of circadian responses to low frequency electromagnetic fields in *Drosophila melanogaster*. *PLoS Genet.* **10**, e1004804. (doi:10.1371/journal.pgen.1004804)
 73. Bae J-E, Bang S, Min S, Lee S-H, Kwon S-H, Lee Y, Lee Y-H, Chung J, Chae K-S. 2016 Positive geotactic behaviors induced by geomagnetic field in *Drosophila*. *Mol. Brain* **9**, 55. (doi:10.1186/s13041-016-0235-1)
 74. Marley R, Giachello CNG, Scrutton NS, Baines RA, Jones AR. 2014 Cryptochrome-dependent magnetic field effect on seizure response in *Drosophila* larvae. *Sci. Rep.* **4**, 5799. (doi:10.1038/srep05799)
 75. Giachello CNG, Scrutton NS, Jones AR, Baines RA. 2016 Magnetic fields modulate blue-light-dependent regulation of neuronal firing by cryptochrome. *J. Neurosci.* **36**, 10 742–10 749. (doi:10.1523/JNEUROSCI.2140-16.2016)
 76. Wong SY, Wei Y, Mouritsen H, Solov'yov IA, Hore PJ. 2021 Cryptochrome magnetoreception: four tryptophans could be better than three. FigShare.